How dry was the Mediterranean during the Messinian salinity crisis?

How dry was the Mediterranean during the Messinian Salinity Crisis?

Iuliana Vasiliev[1,2,†,*], Eveline M. Mezger[3], Stefano Lugli[4], Gert-Jan Reichart[1,3], Vinicio Manzi[5,6], Marco Roveri[5,6]

[1]Department of Earth Sciences, Utrecht University, Budapestlaan 4, 3584 CD, Utrecht, The Netherlands

[2]Faculty of Geology and Geophysics, University of Bucharest, Traian Vuia 6, 020956, Bucharest, Romania

[3]Royal Netherlands Institute of Sea Research, P.O. Box 59, 1790 AB, Den Burg, Texel, The Netherlands

[4] Dipartimento di Scienze Chimiche e Geologiche, University of Modena e Reggio Emilia, Via Campi 103, 41125 Modena, Italy

[5]Dipartimento di Fisica e Scienze della Terra, Università degli Studi di Parma, Parco Area delle Scienze, 157/A, 43124 Parma, Italy

[6]Alpine Laboratory of Paleomagnetism (ALP), Via Madonna dei Boschi 76, Peveragno, 12016 CN, Italy

[†] Now at Senckenberg Biodiversity and Climate Research Centre BiK-F, Senckenberganlage 25, D-60325 Frankfurt am Main, Germany

[*]e-mail: Iuliana.Vasiliev-Popa@senckenberg.de, iuli.iuliana@yahoo.com

Abstract

The Messinian salinity crisis (MSC; 5.97 - 5.33 Ma) is an enigmatic episode of paleoceanographic change, when kilometres-thick evaporite units were deposited in the Mediterranean basin. It is generally accepted that during the MSC interval there was a dry climate in the Mediterranean region. It is difficult to assess how dry the climate was during the MSC because a modern analogue, in size and duration, is absent. Here we reconstruct hydrological changes in the Mediterranean basin during the three main MSC stages using excellently preserved biomarkers. We used the hydrogen isotopic composition of the long chain *n*-alkanes ($\delta D_{n\text{-alkanes}}$) to reconstruct the hydrological changes on the land adjacent to the Mediterranean Sea. Additionally, the δD of long-chain alkenones ($\delta D_{alkenones}$) is used to observe changes in the Mediterranean Sea water source. The $\delta D_{n\text{-alkanes}}$ recorded during the deposition of Primary Lower Gypsum (stage 1) in Monte Tondo indicate a δD of the precipitation comparable to the present-day Mediterranean implying a similar hydrologic regime (indicated by experiments modelling the Miocene-Pliocene transition). Elevated $\delta D_{alkenones}$ values from halite unit (stage 2) of the Realmonte mine are associated with kainite and giant polygons, consistent with presumably high evaporative conditions during halite deposition. The $\delta D_{n\text{-alkanes}}$ recorded during the deposition of Upper Gypsum (stage 3) in Eraclea Minoa indicate a $\delta D_{precipitation}$ typical for much drier settings, similar to the Red Sea region. The relative contribution of the different alkenones from Eraclea Minoa is similar to the one observed in present-day marine settings suggesting that, during stage 3, connections to the open Ocean were likely maintained. However, the $\delta D_{alkenones}$ records during deposition of the evaporites in Eraclea Minoa are similar to those synchronously registered in the Black Sea implying that a similar hydrologic regime, characterized by extended drought, covered large areas of southeastern Europe. Based on the $\delta D_{alkenones}$ similarity and the Paratethys type

of ´Lago Mare´ fauna in the Mediterranean we speculate that the surface water during stage 3 was, at times, derived from the Black Sea.

Keywords: Messinian salinity crisis; Mediterranean Sea; hydrogen isotopes; alkenones; *n*-alkanes; Paratethys

1. Introduction

The Messinian salinity crisis (MSC) of the Mediterranean is one of the paleoceanographic events that had a profound impact, regionally and probably globally in the past ten million years. During this episode, between 5.97 and 5.33 Ma (e.g. Hsü et al., 1973; Krijgsman et al, 1999; Manzi et al., 2013), the paleoenvironment and paleogeography of the circum-Mediterranean was completely modified (Fig. 1). A severe deficit in the water budget of the Mediterranean interrupted the already limited water exchange with both the Atlantic Ocean and the Black Sea (*e.g.* Roveri et al., 2014b) causing the precipitation of an up to 2 km-thick evaporite unit. According to the shallow water-deep basin model (Hsü et al., 1973; Roveri et al., 2014a), evaporite precipitation was associated to a sea level drop in the range of 1500 meters, up to the almost complete desiccation of the Mediterranean. This occurred at the MSC's peak, between 5.60 and 5.55 Ma (Fig. 2), culminating in halite precipitation and marked by the incisions of deep canyons at the Mediterranean margins. Debate is still ongoing regarding the paleoenvironmental conditions of the final 'desiccation' phase. The deep desiccation theory has been recently challenged by new findings suggesting that the depositional facies association and the morphological features, including the canyons, may have been produced without a significant drop of the Mediterranean Sea level (Roveri el al., 2014b, 2016). The presence of marine fish during the latest Messinian powered the hypothesis that fully marine environments existed in several Italian areas well before the Pliocene flooding (Carnevale et al., 2006). At the same time, overspilling of Paratethys waters into the Mediterranean has been argued to explain the presence of brackish water fauna (ostracod and mollusk assemblages of Paratethys affinity) in the 'Lago Mare' (5.55-5.33 Ma) (Suc et al., 1999; Gliozzi et al., 2002; Bertini, 2006; Roveri et al., 2008b, 2008c; Stoica et al., 2016; Marzocchi et al., 2016). For the same time interval, palaeosalinity values in the adjacent Paratethys Sea (Fig. 1) were considered to have varied to a much lesser extent.

New data from two locations in the circum-Black Sea (Vasiliev et al., 2013 and 2015), however, indicate strongly enhanced evaporitic conditions in the Black Sea area of Paratethys as well (Fig. 1). The high evaporative conditions in the Black Sea are expressed in very elevated hydrogen isotope values of biomarker molecules (Vasiliev et al., 2013 and 2015). At that time it is commonly thought that the Mediterranean experienced its major sea-level drawdown phase and a physical link to Paratethys is highly likely (Vasiliev et al., 2013 and 2015). However, the magnitude of hydrological changes and exchanges between Paratethys and Mediterranean basins are virtually unknown. Here we reconstruct hydrological changes in the Mediterranean basin during the MSC using excellently preserved biomarkers extracted from Monte Tondo (Northern Apennines), Realmonte salt mine and Eraclea Minoa (both located on Sicily). These three reference sections cover the principal time intervals of the MSC (Roveri et al., 2014a) respectively: the 'Primary Lower Gypsum' (MSC stage 1; Lower Evaporites), halite unit (MSC stage 2; Lower Evaporites) and 'Upper Gypsum' (MSC stage 3; Upper Evaporites) (Fig. 3). Although these sections have been the subject of extensive studies for more than 60 years (since Selli, 1954), recent advances in the application of hydrogen isotopic values (δD) measured on individual organic components offer a novel, underexploited approach in unravelling fundamental changes in the hydrology of the Mediterranean Sea during the MSC. A single previous study used δD measured on individual sedimentary biomarkers (C_{22} *n*-alkanes and isoprenoids) (Andersen et al., 2001) to successfully track large and rapid hydrographic changes during deposition of the Lower Gypsum. Andersen et al. (2001) estimated that the δD values of the source waters varied by ~100‰ (up to +66‰) over the ~50 kyr studied interval, because of changes in evaporation at low relative humidity. Despite rapid methodological developments in the field of compound specific δD analyses, this method has not been applied further to the Mediterranean MSC. For the present study we use long chain *n*-alkanes (C_{29} and C_{31}) with a distinct odd over even

predominance, as they are principally derived from higher plant waxes and thus reflect the terrestrial environment. We use their δD to reconstruct large scale hydrological changes on the continent adjacent to the Mediterranean Sea over the extent of~640 kyrs, covering the whole MSC interval. Additionally, δD values of long-chain alkenones, produced by haptophyte algae are used to reconstruct the δD of Mediterranean surface water during the MSC. Subsequently, these δD values are exploited to reconstruct changes in the mixing between freshwater/evaporation and inflow of sea water from other sources for the Mediterranean basin. The newly obtained data will be compared and integrated with compound specific δD results already available for the MSC interval from the Paratethys realm (Vasiliev et al., 2013 and 2015). Furthermore, these δD results will be discussed along the available, applied already, climate modelling published results focusing on the Miocene-Pliocene transition in the Mediterranean domain.

2. Stratigraphy of sampled interval

The sedimentary record of the MSC developed over an open marine unit including marls, sapropels and diatomites. The MSC can be separated into three main stages (Roveri et al., 2008a, 2008b and 2014a). Stage 1 (5.97-5.60 Ma) is characterized by the deposition of thick primary selenite gypsum unit (Primary Lower Gypsum; PLG; Lugli et al., 2010) in shallow marginal basins and by organic-rich shale and dolostone deposits in deeper settings. Stage 2 (5.60-5.55 Ma) is characterized by the deposition of a larger variety of evaporites deposits forming the RLG unit (Resedimented Lower Gypsum) including halite and gypsum cumulate deposits, brecciated limestones (‘Calcare di Base’ type 3; Manzi et al., 2011) and clastic gypsum derived from the dismantlement of the PLG unit (Fig. 2). A regional-scale unconformity (Messinian erosional surface) deeply cutting the PLG unit in marginal settings

can be traced up to deeper ones at the base of the RLG unit (Roveri et al., 2008a). Finally, stage 3 (5.55-5.33 Ma) is characterized by the deposition of gypsum (mainly bottom grown selenite and cumulate) interbedded with fine- to coarse-grained terrigenous unit (Upper Gypsum; UG) showing in its uppermost portion the widespread occurrence of a brackish fauna of Paratethyan affinity. There is no known location where the entire MSC interval is continuously outcropping. However, different MSC intervals are well exposed around the Mediterranean. For this study the Monte Tondo quarry, the Realmonte salt mine and the Eraclea Minoa outcrop were selected as they cover the entire MSC time span. These exposures have already been subject to extensive previous research (e.g. Sinninghe Damsteé et al., 1995; Lugli et al., 1999; 2007; 2010; Van Couvering et al., 2000; Bertini, 2006; Manzi et al., 2009; Manzi et al., 2012; Speranza et al., 2013).

2.1 Monte Tondo section – Primary Lower Gypsum unit (MSC stage 1)

The Monte Tondo gypsum quarry, located within the Vena del Gesso basin (along the western Romagna Apennines), contains all the 16 cycles of the PLG, deposited during stage 1 of the MSC (Fig. 2). The 16 precession controlled cycles (sketched in figure 2) are separated by bituminous shales and minor carbonates (marls and stromatolites). Four types of gypsum can be distinguished (Lugli et al., 2007; 2010): giant selenite, massive selenite, banded and branching selenite. Cycles start with shale followed directly by a selenite layer; locally a calcareous stromatolite layer might be present at the base of the gypsum. The bituminous shales may contain leaves, fishes, insects and twig remains. The PLG unit is characterized by a peculiar vertical organization in terms of facies distribution and thickness that has been recognized in different areas of the Mediterranean allowing a basin-scale correlation (Lugli et al., 2010). The lower two cycles are relatively thin and mainly consist of massive selenite

with giant crystals up to more than 2 meters high (giant selenite). Cycles 3 to 5 contain thick beds of vertically orientated massive selenites, grading into banded selenite. Cycle 3 starts with shale, followed by a limestone or stromatolite layer and massive selenite. Cycle 4 starts with a sequence of laminated shale, massive shale and again laminated shale, followed by a succession of both massive and banded selenite. Cycle 5 consists of massive selenite, alternated with thin shales. Cycles 6 to 15 consist of thinner beds of both massive and banded selenite, followed by branching selenite. Cycles 6 and 15 both show a thin stromatolite bed and all cycles are alternated with thin shales. Cycle 16 starts with a shale layer, succeeded by a massive and branching selenite. Pyrite is present in most samples (Sinninghe Damsté et al., 1995).

2.2 Realmonte salt mine – Halite and Resedimented Lower Gypsum unit (MSC stage 2)

The halite unit, underlain and overlain by clastic evaporite deposits, is included in the RLG unit deposited during stage 2 of the MSC (Roveri et al., 2008a and 2014a). It occurs in the deeper parts of the basin whereas coeval primary gypsum cumulates are deposited at the margins (Manzi et al., 2012) (Fig. 2). In the Realmonte mine (southern Sicily) the halite unit is approximately 400 m-thick. From the bottom to the top, it consists of irregular anhydrite and marly mudstone breccia layer up to 2 m thick followed by units A to D (Lugli, et al., 1999). Unit A, up to 50 m thick, contains evenly laminated halite with anhydrite nodules and laminae passing upward to massive halite beds with irregular mudstone bed some decimeters thick. Unit B (approximately 100 m thick) consists of massive even layers of halite inter-bedded with thin kainite laminae, millimeter to centimeter-thick polyhalite spherulite and anhydrite laminae. The upper part contains several kainite layers up to 12 m thick. The 70–80 m thick unit C (), consists of halite 10 to 20 cm thick layers separated by irregular mud

laminae and contains minor polyhalite and anhydrite. Unit D, up to 60 m thick, begins with a gray anhydrite-rich mudstone passing to an anhydrite laminate sequence followed by halite millimeter- to centimeter-thick layers intercalated with anhydrite laminae and decimeter-thick halite beds. Lugli et al. (1999) proposed that these lithologies reflect the shallowing and the desiccation of the evaporitic basin resulting from a possible combination of factors: (1) uplift of the basin floor by thrust activity, (2) simple evaporitic drawdown and (3) a basin-wide drop of the Mediterranean sea level. Manzi et al. (2012) suggest that the well-developed cyclicity characterizing the halite unit is related to annual climate variations and the deposition of the Sicilian Messinian halite could have lasted only a few thousands of years (Roveri et al., 2008).

2.3 Eraclea Minoa section - Upper Gypsum unit (stage 3)

The Eraclea Minoa section is located on the SW coast of Sicily and hosts the global boundary stratotype section and point for the Zanclean stage, marking the beginning of the Pliocene (Van Couvering et al., 2000). The section provides also one of the most complete sedimentary successions of the Upper Gypsum (stage 3; Upper Evaporites) (Manzi et al., 2009). We collected samples from 8 cycles covering the uppermost part of the Miocene and the lower part of the Pliocene (Fig. 2).The cyclic sedimentation starts with an alternation of marls and sandstones, followed by clastic and primary (cumulate facies) and ends with massive selenite (selenite crust, massive selenite separated by thin marl layers, domed selenite and reworked selenite on top of the domes) (Manzi et al., 2009). The section is laying on the RLG unit (Roveri et al., 2008) here consisting of a gypsum turbidite megabed including blocks of PLG in its basal chaotic part, followed by a 2-m thick cumulate gypsum layer suggested to be time equivalent of the halite in Sicily (Manzi et al., 2009). Cycle 1

consists of banded selenite only. Cycle 2 contains thin marl layers, selenite crust and massive selenite. Cycle 3 consists of marls, followed by selenite crust and massive selenite. Cycles 4, 5, the first part of cycle 6 and 7 show the same basic cyclic pattern. Cycle 6 is divided into three parts, of which the last two consist mainly of marls, thin bedded sandstones and are considered as sub-cycles. The interval above cycle 4 contains typical Lago-Mare faunal assemblages (*Melanopsis* and ostracods; Manzi et al., 2009). Above the gypsum bed of cycle 7, a terrigenous interval, including marls and sandstone ('Arenazzolo' sandstone beds), is present; it consists of deltaic deposits that are also present in the lower part of the previous Upper Gypsum cycles (Manzi et al. 2009). The strata deposited during the subsequent Pliocene consist of an alternation of marls and sapropelitic shales known as Trubi formation (Van Couvering et al., 2000).

3. Experimental methods

3.1. Lipid extraction, separation and analyses

In total 41 rock samples (12 from Monte Tondo, 2 from Realmonte mine and 27 from Eraclea Minoa), weighing between 8 and 60 g, were dried and thoroughly ground. Larger samples (i.e. 15-60 g) were extracted using a Soxhlet apparatus with a dichloromethane (DCM) – methanol (7.5:1, v/v) mixture. Smaller samples (up to 15 g) were extracted by accelerated solvent extraction (ASE, Dionex 200) using a DCM-methanol (9:1, v/v) organic solvent mixture at 100°C and 1000 psi. All extracts were rotary – evaporated to near dryness and subsequently further dried under a nitrogen flow. The total lipid extracts were dried over an anhydrous Na_2SO_4 column. Elemental sulfur was removed using activated copper in DCM. Copper flakes were activated with 2M HCl and afterwards rinsed with MilliQ ultra-pure water, methanol and DCM, a treatment repeated up to three times when necessary. An aliquot

of the extract was separated using column chromatography with activated Al_2O_3 as stationary phase by subsequent elution with *n*-hexane/DCM (9:1, v:v), *n*-hexane/DCM (1:1, v:v), and a mixture of DCM/ methanol (1:1, v:v) to obtain the apolar, ketone and polar fractions, respectively. *n*-Alkanes were isolated from the apolar fraction using urea-adduction. To this end, the apolar fraction was dissolved in 200 µl methanol/urea (~10%, H_2NCONH_2, Merck) solution. Subsequently, 200 µl acetone and 200 µl *n*-hexane were added to the solution, frozen (-20ºC) and dried under N_2 flow. Urea crystals were washed with *n*-hexane to remove the non-adductable branched and cyclic compounds and subsequently dissolved in a 500 µl methanol and 500 µl MilliQ ultra-pure water mixture. The *n*-alkanes were extracted from the solution using *n*-hexane. The urea-adduction procedure was repeated up to three times to eliminate non-adductable compounds as much as possible. Alkenones were obtained from the ketone fraction using urea adduction as well, using the same procedure as for the *n*-alkanes.

All fractions were measured using Gas Chromatography/Flame Ionization Detector (GC/FID) first. The *n*-alkanes and alkenones were identified based on mass spectra and their retention times using Gas Chromatography-Mass Spectrometry (GC-MS) on a Thermo-Finnigan Trace DSQ instrument. The fractions (dissolved in *n*-hexane) were injected on-column at 70 ºC (CP-Sil 5CB fused silica column (30 m × 0.31 mm i.d; film thickness 0.1 µm). The oven was set at constant pressure (100 kPa) and then programmed to increase to 130 °C at 20 °C min^{-1}, and then at 5 °C min^{-1} to 320 °C at which it was held isothermally for 10 min.

3.2 Compound-specific hydrogen isotope analyses

Compound-specific hydrogen isotope (δD) compositions of individual *n*-alkanes and alkenones were measured on the adducted fractions using a HP 6890N Gas Chromatograph

(GC) coupled to a Thermo-Finningan Delta Plus XP Isotope Ratio Mass Spectrometer (IRMS). The fractions (dissolved in hexane) were injected on-column at 70 °C, the oven being programmed to increase to 130 °C at 20 °C min^{-1}, and then at 5 °C min^{-1} to 320 °C at which it was held isothermal for 10 min. The film thickness of the CP-Sil 5 column was 0.4 μm and a constant flow of He was used at 1.5 ml min^{-1}. Eluting compounds were pyrolyzed on-line in an empty ceramic tube heated at 1450 °C, which was pre-activated by a 5 min methane flow of 0.5 ml min^{-1}. H_3^+ factors were determined daily on the isotope ratio mass spectrometer and were at any time < 5. H_2 gas with known isotopic composition was used as reference and a mixture of C_{16}–C_{32} *n*-alkanes with known isotopic composition (ranging from −42‰ to −256‰ vs. Vienna Standard Mean Ocean Water (V-SMOW)) was used to monitor the performance of the system (Schimmelman Mixture A and B, Biogeochemical Laboratories, Indiana University). A squalane standard was co-injected with every sample with an average value of −171±3‰, which compared favorably with its offline determined value of −168.9‰. Each fraction was measured between two and five times, depending on the amount of material available.

4. Results

4.1. *n*-Alkane abundance

The apolar fractions contain a series of *n*-alkanes ranging from *n*-C_{16} to *n*-C_{34}, with the long-chain (C_{27}-C_{31}) *n*-alkanes having the highest abundances. These long-chain *n*-alkanes show a strong odd-over-even carbon number predominance (Table 1, Figs 3a, e and k). At some levels the contribution of the shorter chain *n*-alkanes is to some degree higher (Figs 3c and e) although the long-chain (C_{27}-C_{31}) *n*-alkanes clearly dominate the distribution.

There are marked differences between the *n*-alkanes contribution form the samples collected in Monte Tondo and Eraclea Minoa. These differences are in the ranges for the degree of oddity (CPI), expressed as following relation:

$CPI = (((A_{25}+A_{27}+A_{29}+A_{31}+A_{33})/(A_{24}+A_{26}+A_{28}+A_{30}+A_{32})) + ((A_{25}+A_{27}+A_{29}+A_{31}+A_{33})/(A_{26}+A_{28}+A_{30}+A_{32}+A_{34})))*0.5$ where A represents the area under the chromatogram peak for individual *n*-alkanes. The CPI values vary from 3 to 7.9 in Monte Tondo samples while for Eraclea Minoa CPI vary from 1.7 to 3.7 (Table 1).

Although all 41 samples yielded enough lipids to identify the organic compounds (e.g. Fig. 3a and g), since the stable isotope analyses requires much more material to be injected, the extracted amounts were enough for δD analyses in 23 samples only.

4.1.1. n-Alkane δD ratios

The δD of the C_{29} and C_{31} *n*-alkanes (majorly produced by higher terrestrial plants) from Monte Tondo section range between −175‰ and −138‰ (Table 1) and show a strong correlation ($R^2 = 0.92$; Fig. 4), with no appreciable offset between the isotopic values between the compounds. In general, the δD values of the C_{29} *n*-alkane are somewhat less negative than those of the C_{31} *n*-alkane (Fig. 5 and Table 1). From the analyzed Monte Tondo interval, four out of twelve samples contained organically bound sulphur (Sinninghe Damsté et al., 1995) to such a degree that they could not be measured on mass-spectrometers (GC-MS nor GC-IRMS).The extracts from the Realmonte samples contained insufficient *n*-alkanes to allow for δD isotope measurements.

Only six out of the total twenty-seven extracted samples from Eraclea Minoa section contained sufficient long chain *n*-alkanes that could be analyzed for δD of the C_{29} and C_{31} *n*-

alkanes. The δD of the C_{29} and C_{31} *n*-alkanes range between −150‰ and −124‰ (Table 1) and correlate (R^2 = 0.75; Fig. 4). As for Monte Tondo, the δD values of the C_{29} *n*-alkane are somewhat less negative than those of the C_{31} *n*-alkane (Fig. 4 and Table 1).

4.2. Long chain ketones

The ketone fractions show the presence of long-chain unsaturated ethyl and methyl ketones (alkenones) (C_{37}-C_{39}) in the Eraclea Minoa section and the Realmonte samples (Figs 3b, d and h). The alkenone distribution shows a remarkable dominance of the C_{37} ketone, followed closely by the C_{38} ketone and lower but nonetheless appreciable concentrations of the C_{39} ketone. Both C_{37} and C_{38} ketones are dominated by the di-unsaturated components. Alkenones were not detected in Monte Tondo ketone fractions.

4.2.1. Alkenones δD values

The stable hydrogen isotopic composition of the C_{37} and C_{38} alkenones ($\delta D_{alkenone}$) varies markedly between −203‰ to −125‰ (‰ V-SMOW) (Table 2) and show a strong correlation between each other (R^2 = 0.81; Fig. 4). Throughout the record, the δD values of the C_{37} and C_{38} alkenones closely track each other, with the exception of one level in the basal part of Eraclea Minoa, at stratigraphic level of 4.5 m (Table 2).

5. Discussion

5.1. n-Alkanes and their δD isotopic compositions

5.1.1 N-alkanes δD values

The δD ratios of *n*-alkanes reflect primarily the δD composition of precipitation (e.g. Sachse et al., 2004a, 2004b) and are affected to a lesser degree by evapotranspiration (e.g. Sachse et

al., 2006, Polissar and Freeman, 2010). Accordingly, the $\delta D_{n\text{-alkanes}}$ have been successfully used for reconstruction of terrestrial paleo-$\delta D_{precipitation}$ and paleo-evaporation (e.g. Andersen et al., 2001; Pagani et al., 2006; Sachse et al., 2004a; Schefuss et al., 2005; Speelman et al., 2010; Tipple and Pagani, 2010, Feakins et al., 2013; Vasiliev et al., 2013, 2015; Niedermeyer et al., 2016). At all times, the quantitative interpretation of the δD_{water} acknowledges the plant-physiology-induced limitations and, potential soil water evaporation effects marked by differences between the woody vegetation and the grasslands (Smith and Freeman, 2006; Feakins and Sessions, 2010)

The amplitude observed in the $\delta D_{n\text{-alkanes}}$ record of Monte Tondo is approximately 40‰ and in the $\delta D_{n\text{-alkanes}}$ record of Eraclea Minoa approximately 25‰ (Table 1 and Fig. 5). In the composite record of Monte Tondo and Eraclea Minoa the amplitude is 50‰, evolving from lower $\delta D_{n\text{-alkanes}}$ values for the PLG from the Northern Apennines increasing to significantly higher $\delta D_{n\text{-alkanes}}$ during the deposition of Upper Gypsum from Eraclea Minoa (Fig. 5). This overall large range hints towards important changes occurring in the basin hydrology or/and potentially an overall time-shift in the composition of the vegetation between the first and the third MSC stage of the Italian sections. Additionally, these two sites could have been characterized by different vegetation governed by the latitudinal difference (Monte Tondo - PLG from the Northern Apennines versus Eraclea Minoa - Upper Gypsum in Sicily) (Favre et al., 2007).

5.1.2 Comparison with the n-alkanes δD values from present-day records

In the present-day situation, the measured $\delta D_{C29n\text{-alkanes}}$ values from existing lakes located closest to the Sicily section (Lago Grande and Lago Piccolo di Monticchio; Basilicata Region) record values between −169‰ and −180‰ (Sachse et al, 2004). These values are

40‰ to 56‰ more depleted than the $\delta D_{C29n\text{-alkanes}}$ registered in the Upper Gypsum of Eraclea Minoa (−124‰ and −140‰) (Fig. 5). Seemingly, there are no differences between samples of evaporites and marls. Nevertheless, the data set needs to be significantly larger to have attributed a statistical meaning. However, the large offset between the present-day $\delta D_{C29n\text{-alkanes}}$ values and the ones recorded during the deposition of the stage 3 evaporites indicates that conditions were significantly different from today.

The $\delta D_{C29n\text{-alkanes}}$ from the present-day lakes located closest to the Monte Tondo quarry section record values between −159‰ and −167‰ (Sachse et al, 2004). The values obtained from the PLG of Monte Tondo (ranging between −138‰ and −171‰) (Fig. 5) are close to those recorded in present-day Italian lakes (Lago di Massaciuccoli and Lago di Mezzano) (Sachse et al, 2004).

To estimate the δD_{precip} we applied a constant biosynthetic fractionation between source water and *n*-alkane of 157‰ (Sachse et al., 2006; Sessions et al., 1999). Additionally, a different evapo-transpiration enrichment effect was applied for $\delta D_{precipitation}$ calculations (Table 1): (1) of ~30‰ (Sachse et al., 2006) corresponding to modern Western Europe humid conditions and (2) of ~60‰ as described for arid ecosystems (Feakins and Sessions, 2010).

Assuming a Western Europe-like humid environment, the $\delta D_{precipitation}$ values would have varied between –52‰ and –14‰ (Table 1) for Monte Tondo. These values are similar to the $\delta D_{precipitation}$ of around –41‰ to –25‰ recorded presently at stations around Italy (Fig. 1; IAEA, 2001). In the case of prevailing arid conditions (Feakins and Sessions, 2010) the calculated $\delta D_{precipitation}$ would have varied between –85.5‰ and –44‰, values more in line with the Alpine region of Eurasia (IAEA, 2001). The situation is, however, much different for Eraclea Minoa where, assuming a Western Europe-like humid environment, the $\delta D_{precipitation}$ values would have varied between –12‰ and +7‰. Values as high as –8‰ for $\delta D_{precipitation}$

are found in dry coastal areas of the easternmost Mediterranean (e.g. Syria, Jordan, Israel), where excess evaporation affects the region (Fig. 1). In present day configuration, values for $\delta D_{precipitation}$ of +7‰ are registered in the region of the Red Sea – Gulf of Aden and the tropical South Atlantic (Bowen and Revenaugh, 2003). However, for $\delta D_{precipitation}$ to reach values as high as +7‰, the source for the vapors generating the clouds (e.g. Mediterranean during Upper Gypsum deposition) should have been heavily deuterium enriched. This assumption is supported by the deposition of gypsum, largely formed during periods of negative water budget defined by excess evaporation. Assuming a dry climate and woody vegetation the $\delta D_{precipitation}$ values (Feakins and Sessions, 2010) would have varied between –51‰ and –33‰ for the Eraclea Minoa section (Table 1). These values largely overlap with the $\delta D_{precipitation}$ of around –41‰ to –25‰ recorded today around Italy (Fig. 1; IAEA, 2001).

The $\delta D_{n\text{-alkanes}}$ (i.e. $\delta D_{precipitation}$) values for the Upper Gypsum records persistently more δD enriched isotopic values while the values for the $\delta D_{n\text{-alkanes}}$ (i.e. $\delta D_{precipitation}$) of the PLG fluctuate on a significantly larger range (Fig. 5, Table 1).

The values of the $\delta D_{n\text{-alkanes}}$ (i.e. $\delta D_{precipitation}$) for the PLG fluctuate around the expected ones for the present-day environment of the Northern Apennines, where the Monte Tondo section is located. The possible effect related to the latitude difference between the paleogeographic positions of the two sections on the $\delta D_{precipitation}$ could account for ~15‰ difference, similarly to the situation at the present time.

The trend towards higher $\delta D_{precipitation}$ values in the younger part of the record (Upper Gypsum of Eraclea Minoa) can be explained by three different mechanisms, or a combination thereof. First, a change in the dominant water vapor source could offset overall values. Second, distance to the vapor source might have decreased. Third, continental temperatures might have increased. All three proposed mechanisms would strongly influence the

composition of the higher-plant vegetation, which is the source for the long-chain *n*-alkanes and indirectly, alter the recorded $\delta D_{n\text{-alkanes}}$ values.

A potential change in the dominant water vapor source cannot be excluded, situation that could be determined by a deviation of air circulation from being predominantly influenced by westerly's. A significant modification of the distance to the Atlantic moisture source, however, is less likely because palaeogeography did not change considerably between stage 1 and 3. During stage 1 the Mediterranean Sea water level was modulated by the on-off, precession-controlled, connection to the Atlantic (Roveri et al, 2014), while during the final, stage 3 of the MSC an influx of fresher water from Paratethys supplied water to form, at least for a while, the Mediterranean 'Lago Mare' phase. The location and the dimension of the Mediterranean-Paratethys sill during the MSC are unknown but, as already suggested by Marzocchi et al., 2016, for this the mechanism to account for the widespread occurrence of the Paratethyan type of fauna in the marginal Mediterranean marginal basins, the sea level must have been high enough for the Mediterranean Sea to be close to full, but still lower than the Mediterranean-Atlantic sill. Conversely, the world climate during the deposition of the Upper Gypsum was on a warming trend, explaining the higher $\delta D_{n\text{-alkanes}}$ (i.e. δD_{precip}) values (Fig. 5) recorded in Eraclea Minoa. The larger variation recorded in the values of $\delta D_{n\text{-alkanes}}$ (i.e. δD_{precip}) from Monte Tondo is in line with the larger climate variability during the deposition of the PLG.

5.2. Alkenones and their δD isotopic compositions

Alkenones are long-chain ketones synthesized by unicellular haptophyte prymnesiophyte algae, common in the photic zone of the modern ocean (Marlowe et al., 1984; Volkman et al., 1980). Alkenones have been also reported from brackish and freshwater lakes from around

the world (e.g. Volkman et al., 1980; Kristen et al., 2010). Changes in the relative abundance of alkenones with a different degree of unsaturation, expressed in the $U^{k'}_{37}$ index, are commonly used to deduce past sea surface water temperature (Brassell et al., 1986; Prahl & Wakeham, 1987).

The occurrence of alkenones in the studied sections was unexpected because the sedimentary successions were deposited under exceptionally highly saline conditions. Moreover, in the Realmonte and Eraclea Minoa successions, relative abundances of the C_{37}, C_{38} and C_{39} alkenones (Fig. 3b, d and h) mimics closely those present in present-day marine settings. Both $C_{37:2}$ and $C_{38:2}$ alkenones strongly dominate the distribution at Eraclea Minoa and in the Realmonte salt. Therefore, the calculated temperatures based on the $U^{k'}_{37}$ proxy, would suggest high temperatures throughout, at or above the maximum calibration temperature of 28°C. The relative abundance of the $C_{39:2}$ alkenone in the studied sections is somewhat higher than observed in open marine settings and more similar to what has been found in the present-day Black Sea, high alkalinity lakes (Thiel et al., 1997) and both in DSDP core 380A from the central Black Sea and the Taman section from the Black Sea coast (Vasiliev et al., 2013 and 2015). Although high alkalinity lakes show a dominant $C_{37:4}$ alkenone, this compound is absent from the Mediterranean MSC record. The relative abundances of C_{37}, C_{38} and C_{39} are constant throughout the record (Fig. 3b, d and h). Because of the unknown alkenone producer(s) we refrain from calculating temperatures based on the $U^{k'}_{37}$ index.

5.2.1. Alkenones δD values

The δD composition of the alkenones reflects predominantly the δD of the water they live in (Engelbracht and Sachse, 2006; Schouten et al., 2005; Paul, 2002), although values are also influenced by salinity, growth rate (Schouten et al., 2005; Van der Meer et al., 2015; Sachs &

Kawka, 2015) and probably irradiance (Pagani, 2002; Van der Meer et al., 2015). Therefore $\delta D_{alkenone}$ was used as a proxy to reconstruct δD_{water} (Englebrecht and Sachs, 2005; Schouten et al., 2005; Paul, 2002; Schwab and Sachs, 2011), which in turn closely reflects seawater salinity. The existing records of measured δD on alkenones produced in the present day ocean range from approximately −181‰ in the warm Sargasso Sea (at 31º N) (Englebrecht and Sachs 2005) to approximately −200‰ in the temperate Chesapeake Bay (at 43º N) (Schwab and Sachs, 2011). Results on the $\delta D_{alkenones}$ measured for latest 40,000 years from the Mozambique Channel (between Africa and Madagascar) indicate a 20‰ variation (from −180‰ to −200‰), with values of -187‰ for the most recent sediments (~1000 years old) (Kasper et al., 2015). In the recent to present-day Black Sea the values of $\delta D_{alkenone}$ are approximately −225‰, values lower than the rest of the ocean at the same latitude because of the large fresh water input (van der Meer et al., 2008). For the Mediterranean Basin during last interglacial times, the values of $\delta D_{alkenone}$ varied between −185‰ below the S5 sapropel and rapidly decreased to ~−210‰ at the base of the S5 sapropel before it slowly returned to −190‰ (van der Meer et al., 2007).

The results from Eraclea Minoa indicate that the hydrogen isotopic composition of the C_{37} and C_{38} alkenones had a much higher range, showing a variation of more than 75‰ (Table 2 and Figs 4 and 5). Such large offsets signal important changes in Mediterranean Sea hydrology as already indicated by the rhythmic alternation of marl and gypsum layers. These alternations are related to the acknowledged switch between the strong opposite climatic conditions at insolation minima and maxima of a precession cycle. Also remarkable is the fact that relative abundances of C_{37}, C_{38} and C_{39} remain constant throughout the record (Fig. 3b, d, h and Table 2), even for samples with highly contrasting $\delta D_{alkenones}$ values (Figs 3d, h and 4). The compositional stability of the alkenones throughout the record suggests that changes in the stable isotope records reflect actual environmental variability rather than a

change in the algal community composition. The very high values (−125‰ to −146‰) (Table 2, Fig. 5) recorded by the $\delta D_{alkenone}$ observed at Realmonte and Eraclea Minoa indicate extreme drought. In both these sites extreme evaporation is expected because of the deposition of "high" salts (ranging from gypsum to halite and kainite). The levels containing kainite (an evaporite mineral) found in the Realmonte salt mine are indicative for extreme evaporative conditions. One of the levels (RMD at -160m) with an enriched $\delta D_{alkenone}$ value of −166‰ is also rich in kainite (Fig. 5). Subsequently, even more enriched $\delta D_{alkenone}$ (up to −143‰) values are observed at the stratigraphic level where Lugli et al., (1999) described giant salt polygons, evidence for a desiccation surface (Fig. 5). Similarly enriched $\delta D_{alkenones}$ (up to −143‰) values have been previously reported only from the Black Sea, in the Pontian (largely corresponding to MSC interval) in Taman (Vasiliev et al., 2013) and from the same time interval in the central Black Sea (DSDP 42B 380, Fig. 1, Vasiliev et al., 2015).

The heavily enriched (up to −143‰) hydrogen isotopic values measured on the alkenone fractions in the studied of Eraclea Minoa and Realmonte mine sections require extraordinary conditions affecting the latest Miocene Mediterranean Sea. The conditions seem to be much different from the recent-times Mediterranean Sea where, since the last interglacial, the recorded $\delta D_{alkenone}$ varied between −185‰ and −210‰ (van der Meer et al., 2007). Regardless of the applied calibration (Englebrecht and Sachs, 2005; Paul, 2002; Schouten et al., 2005; Schwab and Sachs, 2011; van der Meer et al., 2015; Sachs & Kawka, 2015), our $\delta D_{alkenone}$ results indicate extreme evaporation prevailing during stage 2 (halite) and 3 (Upper Gypsum). Still, similarly to alkenone based SST reconstructions (Prahl and Wakeham, 1987), there are limitations when calculating δD_{water} from $\delta D_{alkenone}$, since e.g. the species on which the calibration is based on did not exist during the late Miocene (*Emiliania huxleyi* and *Gephyrocapsa oceanica)*. Therefore, we here consider only relative changes in δD_{water} (Fig. 5).

5.3. Comparison and integration of the δD data into the existing models

Evaluation of the role of the Mediterranean's freshwater fluxes in controlling both its environmental evolution and exchange through its gateways is in its early stages being hampered by inadequate rainfall datasets as well as by model-data mismatch on temporal as well as spatial scales (Flecker et al, 2015). Most model data cover the entire MSC event, without distinction between the three specific stages of the MSC. Even more, more complex models like isotope-enabled general circulation models (GCM) are absent for the MSC events of the Mediterranean. Therefore we discuss our δD data in relation to the existing models of hydroclimate analysis available for the Late Miocene of the Mediterranean.

Results from simulations on an atmosphere-only GCM indicate an increase in net precipitation during the Late Miocene, causing increased river runoff around three times greater than today as a consequence of increased input from North African rivers feeding the Eastern Mediterranean (Gladstone et al., 2007). Many more rivers were thought to have transported water from the south (Griffin, 1999) as a result of a stronger African summer monsoon (Marzocchi et al., 2015; Gladstone et al., 2007). However, the same model predicts a smaller net hydrologic budget (river discharge plus precipitation minus evaporation) than for present day. At precession scale, wetter periods in the Mediterranean region may also have resulted from enhanced wintertime storm track activity in the Atlantic and associated increased precipitation (Kutzbach et al., 2014). Our δD data from the stage 3 of the MSC (Eraclea Minoa section) would suggest drier conditions than present-day, in line with the predicted smaller net hydrologic budget of Gladstone et al. (2007) despite the three times higher modelled runoff. Gladstone et al. (2007) model focuses on a comparison between the situation during Late Miocene, period of time covering the entire MSC, and the present-day

conditions. The model does not distinguish among the three MSC stages and therefore we cannot relate to our three δD data sets, specific to the three different stages of the MSC.

The vegetation experiments did not show dramatic climate changes at the margins of the Mediterranean basin during the MSC (Schneck et al., 2010). Our $\delta D_{n\text{-alkanes}}$ data from the Monte Tondo section deposited during stage 1 of the MSC indicate a $\delta D_{precipitation}$ similar to the present–day Mediterranean regime. Therefore, the precipitations would not have been a factor determining vegetation changes in the Mediterranean domain.

Considering that our research provides only the second dataset on the δD related proxies on the Mediterranean MSC we would favour more δD data acquisition at a precession scale. The sampling and data acquisition could be concentrated on resolving 'the inadequate rainfall data as well as model-data mismatch on temporal as well as spatial scales' (Flecker et al., 2015). The spatial coverage should be concentrated on the west (wetter) to east (dryer) transect of the Mediterranean as well on the latitudinal transect from the north (covered by forest now) to south (dry conditions type of vegetation). The temporal coverage would concentrate specifically on the three stages of the MSC, on the onset, development and the demise. The much different hydrological conditions assumed for the three stages requires detailed data acquisition, to be used as data-check in further modelling exercises of complex models like isotope-enabled general circulation models.

6. Data integration on composite of Monte Tondo, Realmonte and Eraclea Minoa

6.1. δD results on biomarkers from the Mediterranean MSC

The $\delta D_{n\text{-alkanes}}$ and $\delta D_{alkenones}$ results are in line with the presence of vast accumulations of evaporites, indicators for dry environmental conditions (Fig. 5, Tables 1 and 2). However, the δD composition of the individual biomarkers indicates that more extreme conditions were

characterizing the environment during stage 3 in comparison to stage 1. Regardless the applied evapo-transpiration enrichment effect (humid of dry environment-), the $\delta D_{n\text{-alkanes}}$ results indicate that much dryer conditions than today were affecting the Mediterranean between 5.55 and 5.32 Ma (Fig, 5). Dryer conditions were also inferred by Bertini (2006), who indicate an expansion of the open vegetation including the northward migration of *Lygeum* (a steppe element), occurring at about 5.5 Ma. Additionally, at Eraclea Minoa, Londeix et al., (2007) observed the absence of fresh water algae inputs and very low amount in trees requiring humid conditions. Our higher $\delta D_{n\text{-alkanes}}$ and the existing palynology are also in line with the results of the enriched $\delta D_{alkenones}$ from Eraclea Minoa and Realmonte indicating that more evaporation relative to precipitation was affecting the Mediterranean water surface during the MSC climax and Upper Gypsum deposition (Fig. 5). Our enriched $\delta D_{n\text{-alkanes}}$ and $\delta D_{alkenones}$ suggesting dryer conditions are also sustained by preliminary δD and $\delta^{18}O$ values of the crystallization water of gypsum from Eraclea Minoa stage 3 (Evans et al., 2016).

The $\delta D_{n\text{-alkanes}}$ results from Monte Tondo (deposited during stage 1 of the MSC) are largely varying around the values expected for the present-day configuration (latitude and position within the Mediterranean) suggesting a precipitation pathway similar to today. However, there are also levels $\delta D_{n\text{-alkanes}}$ values, typical for drier conditions (Fig. 5). Intense evaporation at low relative humidity was also suggested by Andersen et al., (2001). These authors calculated deuterium enriched isotope compositions of the Mediterranean waters of, sometimes reaching, +66‰ (typical for highly evaporative settings).

Recurrent connection to the Atlantic was frequently used to explain the quasi-marine $^{87}Sr/^{86}Sr$ values recorded during deposition of the PLG (e.g. Müller and Mueller, 1991; Flecker and Ellam, 1999; Lugli et al., 2010; Roveri et al., 2014a). Natalicchio et al. (2014) found that in the northernmost offshoot of the Mediterranean Basin, gypsum did not form just

from pristine evaporated seawater, but rather from a mix of seawater and Ca_{2+} and SO_4^{2-} enriched nonmarine waters. Additionally, the presence of open marine planktic biota (diatoms and rare foraminifers) in northern Mediterranean sub-basins further advocated for a connection to a marine water body during stage 1 (Dela Pierre et al., 2014). Therefore, the presence of alkenone producers (unicellular haptophyte prymnesiophyte algae) was expected at least during prolonged marine intermittent connectivity defining the deposition during the stage 1 of the MSC. Unexpectedly, no alkenones were found in the PLG from the Monte Tondo section. The absence of alkenones during stage 3 can be related to: 1) absence of alkenone producers 2) lack of their preservation and/or 3) chemical alteration determined by the sulphurisation of the organic matter (Sinninghe Damsté et al., 1995). We favor the latter because: 1) unicellular haptophyte prymnesiophyte algae (the alkenone producers) are expected during prolonged connection to open marine environments typical for the stage 1; 2) alkenones are some of the most resistant biomarkers over geological time and 3) sulphurisation of organic matter is a process frequently affecting anoxic/disoxic sedimentation of the euxinic shales (Sinninghe Damsteé et al., 1995).

6.2. Comparison between δD results on biomarkers from the Mediterranean and the Paratethys during MSC

6.2.1. Mediterranean – Paratethys correlation

Overspilling of the Paratethys into the Mediterranean during the latest Messinian (Cita et al., 1978; Orszag-Sperber, 2006; Roveri et al., 2008) is acknowledged by the presence of a Paratethys type of biota found in the Lago Mare facies deposits (Suc et al., 1999; Gliozzi et al., 2002; Bertini, 2006; Roveri et al., 2008b; 2008c; Grossi et al., 2008). However, the exact relationship between the Mediterranean and Paratethys during the MSC was for a long time

hampered by the inadequate stratigraphic correlations and insufficiently robust age control on the Paratethys deposits. Integrated magnetobiostratigraphic studies performed in the past 10 years on the Paratethys Messinian sedimentary successions revealed that the entire MSC interval in the Paratethys is included in the Pontian (Vasiliev et al., 2004, 2011; Krijgsman et al., 2010).

6.2.2. Changes marking the pre-onset of the MSC

The onset of the MSC in the Mediterranean post-dates the Maeotian–Pontian transition occurring at 6.04±0.01 Ma in the Paratethys (Krijgsman et al., 2010; Vasiliev et al., 2011). The base of the Pontian is marked by an interval containing marine foraminifera suggesting that a marine flooding event took place in the Paratethys, probably resulting from a connection with the Mediterranean (Stoica et al., 2013). The connection with the marine Mediterranean is also suggested by the $\delta D_{alkenone}$ recorded at two locations in the Black Sea (in Taman land based sections and DSPD 42B 380 Hole); these $\delta D_{alkenone}$ values (−220‰ and −200‰ respectively) are close to those recorded in the present-day Black Sea (−225‰), a restricted marine basin connected to the ocean via the Mediterranean (Vasiliev et al., 2013). The $\delta D_{C29n\text{-alkanes}}$ (i.e. δD_{precip}) recorded at the Maeotian–Pontian transition in both Taman land based sections and the DSDP 42B 380 Hole register values typical for the latitudinal and paleogeographic position similar to the present day situation (i.e. intracontinental marine basin).

6.2.3. Changes during stage 1

The $\delta D_{n\text{-alkanes}}$ results from Monte Tondo are largely suggesting a precipitation pathway similar, at times, to today. There are also levels where the $\delta D_{C29n\text{-alkanes}}$ values were up to −135‰ more enriched, probably induced by drier conditions (Fig. 5). These values are recognized in the branching and banded selenite facies that have been considered to mark the

acme of aridity and show higher $^{87}Sr/^{86}Sr$ values (Lugli et al., 2010), thus suggesting a deposition during higher oceanic input. Drier conditions were also inferred by Andersen et al., 2001, who, using the $\delta D_{C22 n\text{-alkanes}}$ values calculated the deuterium enriched isotope composition (up to values of +66‰) of the Mediterranean waters. Such values are indicative for highly evaporative conditions, at least during the ~50 kyr interval covered by the samples. More comparative information comes from the adjacent Black Sea domain (Fig. 6). The values of the $\delta D_{C29 n\text{-alkanes}}$ recorded from Taman and DSDP 42B Leg 380 vary around −180‰ to −200‰. These values are lower than those recoded in the period preceding the onset of the MSC in the Black Sea. During the deposition of the PLG in the Mediterranean, the $\delta D_{alkenones}$ values from the Black Sea basin (the Taman section and the DSPD 42B Hole 380 provided the new ages models of Chang et al., 2014 and van Baak et al., 2015) are recording a shift at ~5.8 Ma from values typical for present-day Black Sea (−200‰) to values more enriched than any existing record (−145‰) (Fig. 6).

6.2.4. Changes during stage 3

The corroborated $\delta D_{n\text{-alkanes}}$ and $\delta D_{alkenones}$ results from Eraclea Minoa are suggesting significantly dryer conditions in Sicily during the deposition of the Upper Gypsum (stage 3). The values of the $\delta D_{C29 n\text{-alkanes}}$ are reaching highly enriched values, up to −125‰. The most enriched values are recorded in the gypsum samples, whereas the less enriched values are from the marls; among the latter, two samples show values similar to those of modern lakes. The onshore Upper Gypsum $\delta D_{n\text{-alkanes}}$ are also more enriched when compare to their alleged time equivalent deposits of the DSDP 42B 380 borehole of the Black Sea (−180‰). This is expected, since the Black Sea record originates from a more intracontinental position that generally translates into more depleted values for the $\delta D_{precipitation}$ used by the vegetation resulting in more depleted $\delta D_{C29 n\text{-alkanes}}$. The values of the $\delta D_{alkenones}$ vary between values suggesting evaporative conditions (−125‰) and values suggesting more present-day values

in the Mediterranean (−203‰). Lower values (of −200‰) are also recorded in the DSDP 42 B 380 Hole. A physical link between the Mediterranean and Paratethys is likely, justifying the similar $\delta D_{alkenones}$ values as already inferred from the presence of Paratethys type of fauna in the Upper Gypsum of Eraclea Minoa. Noteworthy is that, in both Mediterranean and Paratethys domain, there is a 30 to 40‰ enrichment in the $\delta D_{n\text{-alkanes}}$ (i. e. $\delta D_{precipitation}$) indicating concurrent changes in both Mediterranean and Paratethys during the latest phase of the MSC.

7. Conclusions

The δD results on specific biomarkers from the composite record covering the entire MSC interval in the Mediterranean Sea are converging towards large environmental changes. These δD data in relation to those existing in adjacent Paratethys realm (Fig. 6) are indicating:

1) The $\delta D_{n\text{-alkanes}}$ recorded during MSC stage 1 indicate a $\delta D_{precipitation}$ similar to the present-day Mediterranean hydrologic regime (Fig. 6 b and c). Only at some levels, the $\delta D_{n\text{-alkanes}}$ (i.e. $\delta D_{precipitation}$) are more enriched suggesting more arid/warm conditions or a proximity of the vapor source. However, in conjunction with the existing $\delta D_{C22n\text{-alkanes}}$, significantly drier conditions were to be expected during stage 1. Proximity of the vapor source as the cause for the more enriched values cannot be excluded although, during stage 1, the Mediterranean is considered to have experienced on-off connections to the Atlantic, modulated by precession.
2) The absence of the alkenones for the entire PLG unit is most likely related to sulphurisation of the organic matter. Noteworthy is that, at the moment, there is no rock record from the deepest Mediterranean basin for the stage 1, a time when PLG was deposited in the marginal settings. Therefore, because of absence of offshore data, we

refrain stating that in the stage 1 evaporite were deposited only in the shallow part of the basin. This can be explained by the presence of anoxic environments at depth that hampered the deposition of the gypsum (Lugli et al., 2010; De Lange & Krijgsman, 2010). The anoxia extended in the photic zone as indicated by the presence of isorenieratane, a biomarker produced by anaerobic green sulphur bacteria topped up by the strong water column stratification as shown by the occurrence of the gammacerane produced by bacterivorous ciliates (Sinninghe Damste, 1995).

3) Enriched $\delta D_{alkenones}$ from the Realmonte mine (stage 2) are associated with kainite (mineral forming under extreme evaporation conditions) and giant polygons (evidence of an exposure surface). These observations combined favor the conclusion that, at least at some moments, the Mediterranean Sea level dropped down because of excess evaporation.

4) All the $\delta D_{n\text{-alkanes}}$ values recorded during stage 3 of the MSC indicate a $\delta D_{precipitation}$ much different from the present-day Mediterranean hydrological regime (Fig. 6 a). The values are typical for much drier settings, like Red Sea – Gulf of Aden, region with extreme evaporation rates. In both Mediterranean and Paratethys domain, there is a 30 to 40‰ enrichment in the $\delta D_{n\text{-alkanes}}$ (i. e. $\delta D_{precipitation}$) indicating concurrent changes in both Mediterranean and Paratethys during the latest phase of the MSC.

5) The relative contribution of alkenones in the Upper Gypsum of Eraclea Minoa is similar to the present-day marine setting (although the principal present-day Ocean alkenone producers – *Emiliania huxleyi* and *Gephyrocapsa oceanica* – did not exist at that time). Therefore, we may suggest two different possible scenarios. i) One of them would imply the existence of a connection to the open Ocean during stage 3, most probably at insolation minima, that could have provided the ions needed for the precipitation of the evaporites (Manzi et al., 2009; Roveri et al., 2014b). ii) Alternatively, since the relative

contribution of the C_{37}, C_{38} and C_{39} alkenones appears similar to the one of the alkenones extracted from samples originating from the Black Sea (part of the Paratethys), we could also speculate that the alkenone producers were common for the Mediterranean and Black Seas, thus it was at least an outflow of Black Sea (i.e. Paratethys) waters into the Mediterranean, paving the way for Paratethys type of 'Lago Mare' fauna.

6) There is no data of $\delta D_{alkenones}$ from the open Ocean settings deposited during the upper most Miocene. Therefore, we can only compare our Mediterranean MSC $\delta D_{alkenones}$ record with the existing ones form the equivalent in time $\delta D_{alkenones}$ of the Black Sea (DSDP 42B Hole 380 and Taman peninsula). The $\delta D_{alkenones}$ recorded during stage 3 from Eraclea Minoa are similar to those equivalents in time from the Black Sea records. Because of this similarity we speculate that the surface water from the Upper Gypsum must be derived from the Black Sea, consistent with Paratethys water inflow into the Mediterranean. Alternatively, the Mediterranean and Paratethys could have been exchanging surface water at insolation maxima.
7) The δD on biomarkers could be the method to be used to finally understand the extraordinary hydrological changes affecting the Mediterranean region during the MSC under the provision that increased resolution of $\delta D_{biomarker}$ data will be produced

Acknowledgements

We are grateful to ITALKALI and the director of the Realmonte mine for the permission to sample. IV thanks to Wout Krijgsman for inspiring discussions on the extraordinary changes during MSC. This research was financially supported by the Netherlands Earth and Life Sciences Foundation (ALW) with support from the Netherlands Organization for Scientific Research (NWO) via a Veni grant of IV. This research was also supported by a grant of the Romanian National Authority for Scientific Research and Innovation, CNCS – UEFISCDI,

project number PN-II-RU-TE-2014-4-0050 awarded to IV. This work was carried out under the program of the Netherlands Earth System Science Centre (NESSC). IV thanks to Sarah Feakins and the anonymous reviewer for the constructive comments that improved the manuscript.

References

Andersen, N., Paul, H.A., Bernasconi, S.M., McKenzie, J.A., Behrens, A., Schaeffer, P., Albrecht, P. 2001. Large and rapid climate variability during the Messinian salinity crisis: Evidence from deuterium concentrations of individual biomarkers. Geology, 29, 799–802.

Bertini, A., 2006. The Northern Apennines palynological record as a contribution for the reconstruction of the Messinian palaeoenvironments. Sedimentary Geology, 188, 235-258.

Brassell, S.C., Eglinton, G., Marlowe, I.T., Pflaumann, U., Sarnthein, M., 1986. Molecular stratigraphy e a new tool for climatic assessment. Nature, 320, 129-133.

Carnevale, G., Landini, W., Sarti, G., 2006. Mare versus Lago-mare: marine fishes and the Mediterranean environment at the end of the Messinian Salinity Crisis. Journal of the Geological Society, 163, 75-80.

Chang, L., Vasiliev, I., Van Baak, C.G.C., Krijgsman, W., Dekkers, M.J., Roberts, A.P., 2014. Identification and environmental interpretation of diagenetic and biogenic greigitein sediments: A lesson from the Messinian Black Sea, Geochemistry, Geophysics, Geosystems, 15, 3612–3627.

Dela Pierre, F., Clari, P., Natalicchio, M., Ferrando, S., Giustetto, R., Lozar, F., Lugli, S., Manzi, V., Roveri, M., Violanti, D., 2014. Flocculent layers and bacterial mats in the mudstone interbeds of the Primary Lower Gypsum unit (Tertiary Piedmont basin, NW Italy): Archives of palaeoenvironmental changes during the Messinian salinity crisis. Marine Geology, 355, 71-87.

De Lange, G.J., Manzi, V., Lugli, S., Roveri, M. and Charlotte, B., 2009. A new facies model for the Upper Gypsum of Sicily (Italy): chronological and palaeoenvironmental

constraints for the Messinian salinity crisis in the Mediterranean, Sedimentology 56, 1937-1960.

De Lange, G.J., Krijgsman, W., 2010. Messinian Salinity Crisis: a novel unifying shallow gypsum/ deep dolomite formation mechanism, Marine Geology, 275, 273-277.

Eglinton, G., Hamilton, R.J., 1967. Leaf Epicular Waxes. Science, 156, 1322-1335.

Englebrecht, A.C., Sachs, J.P., 2005. Determination of sediment provenance at drift sites using hydrogen isotopes and unsaturation ratios in alkenones. Geochimica et Cosmichimica Acta, 69, 4253-4265.

Evans, N.P., Gázquez, F., McKenzie, J.A., Chapman, H.J.(1), Hodell, D.A., 2016. Constraining the origin of the Messinian gypsum deposits using coupled measurement of $\delta^{18}O$/ δ D in gypsum hydration water and salinity of fluid inclusions, Geophysical Research Abstracts, Vol. 18, EGU 2016-10169-2.

Favre, E., François, L., Fluteau, F., Cheddadi, R. , Théveno, L.; Suc, J.-P. 2007, Messinian vegetation maps of the Mediterranean region using models and interpolated pollen data. Cartes de végétation de la région méditerranéenne au Messinien d'après les modèles et les données polliniques interpolées, Geobios, 40, 433–443.

Feakins, S.J., Sessions, A.L., 2010. Controls on the D/H ratios of plant leaf waxes in an arid ecosystem. Geochimica et Cosmichimica Acta, 74, 2128-2141.

Feakins, S. J., Levin, N.E., Liddy, H.M. Sieracki, A. I. Eglinton, T.I., Bonnefille, R., 2013. Northeast African vegetation change over 12 m.y. Geology, 41, 295-298.

Flecker, R., Krijgsman, W., Capella, W., de Castro Martíns, C., Dmitrieva, E., Mayser, J.P., Marzocchi, A., Modestu, S., Lozano, D.O., Simon, D., Tulbure, M., van den Berg, B., van der Schee, M., de Lange, G., Ellam, R., Govers, R., Gutjahr, M., Hilgen, F., Kouwenhoven, T., Lofi, J., Meijer, P., Sierro, F.J., Bachiri, N., Barhoun, N., Alami, A.C., Chacon, B., Flores, Jose A., Gregory, J., Howard, J., Lunt, D., Ochoa, M., Pancost, R.,

Vincent, S., Yousfi, M.Z., 2015, Evolution of the Late Miocene MediterraneanAtlantic gateways and their impact on regional and globalenvironmental change, Earth Science Reviews, 150, 365-392.

Gladstone, R., Flecker, R., Valdes, P., Lunt, D., Markwick, P., 2007, The Mediterranean hydrologic budget from a Late Miocene global climate simulation. Palaeogeography, Palaeoclimatology, Palaeoecology 251, 254–267.

Gliozzi E., Cipollari P., Cosentino D., 2002. The Messinian Lago-Mare event in central Italy: palaeogeographical reconstruction using geological data and ostracods assemblages. GeoInstitute, Spec. Publ. 26: 153-168.

Griffin, D.L., 1999. The late Miocene climate of Northeastern Africa: unravelling the signals in the sedimentary succession. Journal of the Geological Society of London 156, 817–826.

Hilgen, F.J., Kuiper, K.F., Krijgsman, W., Snel, E., Van der Laan, E., 2007. Astronomical tuning as the basis for high resolution chronostratigraphy: the intricate history of the Messinian salinity crisis. Stratigraphy, 1, 231–238.

Hsü, K.J., Ryan, W.B.F., Cita, M.B., 1973. Late Miocene desiccation of the Mediterranean. Nature, 242, 240-244.

Kutzbach, J.E., Chen, G., Cheng, H., Edwards, R.L., Liu, Z., 2014. Potential role of winter rainfall in explaining increased moisture in the Mediterranean and Middle East during periods of maximum orbitally-forced insolation seasonality. Climate Dynamics 42, 1079–1095.

IAEA, 2001. GNIP Maps and Animations, International Atomic Energy Agency, Vienna. http://isohis.iaea.org.

Kasper, S., van der Meer, M.T.J., Castañeda, I.S., Tjallingii, R., Brummer, G.J. A. Sinninghe Damsté, J.S., Schouten, S., 2015. Testing the alkenone D/H ratio as a paleoindicator

of sea surface salinity in a coastal ocean margin (Mozambique Channel), Organic Geochemistry, 78, 62-68.

Krijgsman, W., Hilgen, F.J., Raffi, I., Sierro, F.J. and Wilson, D.S., 1999. Chronology, causes and progression of the Messinian salinity crisis. Nature, 400, 652-655.

Krijgsman, W., Stoica, M., Vasiliev, I. and Popov, V.V., 2010. Rise and fall of the Paratethys Sea during the Messinian Salinity Crisis. Earth and Planetary Science Letters, 290: 183-191.

Londeix, L., Benzakour, M., Suc, J. P., & Turon, J. L. 2007. Messinian palaeoenvironments and hydrology in Sicily (Italy): the dinoflagellate cyst record. Geobios, 40, 233-250.

Lugli, S., Bassetti, M.A., Manzi, V., Barbieri, M., Longinelli, A., Roveri, M., 2007. The Messinian 'Vena del Gesso' evaporates revisited: characterization of isotopic composition and organic matter, Geological Society of London 285, 179-190.

Lugli, S., Manzi, V., Roveri, M., Schreiber, B.C., 2010. The primary Lower Gypsum in the Mediterranean: A new facies interpretation for the first stage of the Messinian salinity crisis, Palaeogeography, Palaeoclimatology, Palaeoecology 297, 83-99.

Lunt, D.J., Flecker, R., Valdes, P.J., Salzmann, U., Gladstone, R., Haywood, A.M., 2007, The Mediterranean hydrologic budget from a Late Miocene global climate simulation, Palaeogeography, Palaeoclimatology, Palaeoecology, 251, 254–267.

Manzi, V., Lugli, S., Roveri,M., Schreiber, B.C., 2009. A new facies model for the Upper Gypsum (Sicily, Italy): chronological and palaeoenvironmental constraints for the Messinian salinity crisis in the Mediterranean. Sedimentology 56, 1937–1960.

Manzi, V., Gennari, R., Lugli, S., Roveri, M. and Schreiber, B.C., 2011. The Messinian "Calcare di Base" (Sicily, Italy) revisited. Geological Society of America Bulletin, 123, 347-370.

Manzi, V.,Gennari, R., Lugli, S., Roveri, M., Scafetta, N., Schreiber, B. C., 2012. High-frequency cyclicity in the Mediterranean Messinian evaporites: evidence for solar-lunar climate forcing. Journal of Sedimentary Research, 82, 991–1005.

Manzi, V., Gennari, R., Hilgen, F., Krijgsman, W., Lugli, S. Roveri, M., Sierro, F.J., 2013. Age refinement of the Messinian salinity crisis onset in the Mediterranean. Terra Nova, 315-322.

Marlowe, I.T., Green J. C., Neal A. C., Brassell S. C., Eglinton G., Course P. A., 1984. Long-chain (n-C_{37-39}) alkenones in the Prymnesiophyceae. Distribution of alkenones and other lipids and their taxonomic significance. British Phycological Journal, 19, 203-216.

Marzocchi, A., Flecker, R., Van Baak, C.G.C., Lunt, D.J. and Krijgsman, W., 2016. Mediterranean outflow pump: An alternative mechanism for the Lago-mare and the end of the Messinian Salinity Crisis, Geology, 44, 523-526.

Müller, D.W., Mueller, P.A., 1991. Origin and age of the Mediterranean Messinian evaporites: implications from Sr isotopes, Earth and Planetary Science Letters 107, 1-12.

Natalicchio, M., Dela Pierre, F., Lugli, S., Lowenstein, T. K., Feiner, S.J, Ferrando, S., Manzi, V., Roveri, M., Clari, P., 2014. Did Late Miocene (Messinian) gypsum precipitate from evaporated marine brines? Insights from the Piedmont Basin (Italy), Geology, 42, 179-182.

Niedermeyer, E. M., Chase, B., Gleixner, G., Mulch, A., 2016. Southwestern African climate change during Heinrich Stadial 1 inferred from plant wax d13C and dD from rock hyrax middens. Quaternary International, 404, Part B, 202, doi: 10.1016/j.quaint.2015.08.181

Pagani, M., 2002. The alkenone - CO_2 proxy and ancient atmospheric carbon dioxide. Philosophical Transactions of the Royal Society of London, 360, 609-632.

Pagani, M. et al., 2006. Arctic hydrology during global warming at the Palaeocene/Eocene thermal maximum. Nature, 442, 671-675.

Paul, H.A., 2002. Application of novel stable isotope methods to reconstruct peleoenvironments: Compound-specific hydrogen isotopes and pore-water oxygen isotopes. Ph. D. Thesis, Swiss Federal Institute of Technology, Zurich, 141 pp.

Polissar, P.J., Freeman, K.H., 2010. Effects of aridity and vegetation on plant-wax dD in modern lake sediments. Geochimica et Cosmichimica Acta, 74, 5785-5797.

Prahl, F.G., Wakeham, S.G., 1987. Calibration of unsaturation patterns in long-chain ketone compositions for paleotemperature assessment. Nature, 330, 367-369.

Roveri, M., Lugli, S., Manzi, V., Schreiber, B.C., 2008a. The Messinian Sicilian stratigraphy revisited: toward a new scenario for the Messinian salinity crisis. Terra Nova 20, 483–488.

Roveri, M., Bertini, A., Cosentino, D., Di Stefano, A., Gennari, R., Gliozzi, E., Grossi, F., Iaccarino, S.M., Lugli, S., Manzi, V., Taviani, M., 2008b. A high-resolution stratigraphic framework for the latest Messinian events in the Mediterranean area. Stratigraphy 5, 323–342.

Roveri, M., Manzi, V., Gennari, R., Iaccarino, S.M., Lugli, S., 2008c. Recent advancements in the Messinian stratigraphy of Italy and their Mediterranean-scale implications, Bollettino della Societa Paleontologica Italiana, 47 (2), 71-85.

Roveri, M., Flecker, R., Krijgsman, W., Lofi, J., Lugli, S., Manzi, V., Sierro, F.J., Bertini, A., Camerlenghi, A., De Lange, G., Govers R., Hilgen F.J., Hübscher, C., Meijer, P.T., and Stoica, M., 2014a. The Messinian Salinity Crisis: Past and future of a great challenge for marine sciences, Marine Geology, 352, 25-58.

Roveri, M., Lugli, S., Manzi, V., Gennari, R., Schreiber, B.C., 2014b. High-resolution strontium isotope stratigraphy of the Messinian deep Mediterranean basins: implications for marginal to central basins correlation. Marine Geology 349, 113–125.

Roveri, M., Manzi, V., Bergamasco, A., Falcieri, F., Gennari, R., Lugli, S., 2014c. Dense shelf water cascading and Messinian canyons: a new scenario for the Mediterranean salinity crisis. American Journal of Science, 314, 751-784.

Roveri, M., Gennari, R., Lugli, S., Manzi, V., Minelli, N, Reghizzi M., Riva, A., Rossi, M.E. Schreiber, B.C., 2016. The Messinian salinity crisis: open problems and possible implications for Mediterranean petroleum systems. Petroleum Geoscience, 22, 283-290.

Sachs, J.P., Kawka, O.E., 2015. The Influence of Growth Rate on $^{2}H/^{1}H$ Fractionation in Continuous Cultures of the Coccolithophorid *Emiliania huxleyi* and the Diatom *Thalassiosira pseudonana*. PloS ONE 10(11): e0141643. doi:10.1371/journal.pone.014164.

Sachse, D., Radke, J., Gaupp, R., Schwark, L., Lüniger, G., Gleixner, G., 2004a. Reconstruction of palaeohydrological conditions in a lagoon during the 2nd Zechstein cycle through simultaneous use of δD values of individual *n*-alkanes and $d^{18}O$ and $\delta^{13}C$ values of carbonates. International Journal of Earth Sciences, 93, 554–564.

Sachse, D., Radke, J., Gleixner, G., 2004b. Hydrogen isotope ratio of recent lacustrine sedimenatry n-alkanes record modern climate variability. Geochimica et Cosmichimica Acta, 68, 4877-4889.

Sachse, D., Radke, J., Gleixner, G., 2006. δD values of individual *n*-alkanes from terrestrial plants along a climatic gradient - implications for the sedimentary biomarker record. Organic Geochemistry, 37, 469–483.

Sawada, K., Handa, N., Shiraiwa, Y., Danbara, A., Montani, S., 1996. Long-chain alkenones and alkyl alkenoates in the coastal and pelagic sediments of the northwest North Pacific, with special reference to the reconstruction of *Emiliania huxleyi* and *Gephyrocapsa oceanica* ratios Organic Geochemistry, 24, 751–764.

Schefuss, E., Schouten, S., Schneider, R.R., 2005. Climatic controls on central African hydrology during the past 20,000 years. Nature, 437, 1003-1006.

Schneck, R., Micheels, A., Mosbrugger, V., 2010. Climate modelling sensitivity experiments for the Messinian Salinity Crisis. Palaeogeography, Palaeoclimatology, Palaeoecology, 286, 149–163.

Schouten, S., Ossebaar, J., Schreiber, K., Kienhuis, M. V. M., Langer, G., Bijma, J., 2005. The effect of temperature and salinity on the stable hydrogen isotopic composition of long chain alkenones produced by Emiliania huxleyi and Gephyrocapsa oceanica. Biogeosci. Discusions, 2, 1681–1695.

Schwab, V., Sachs, J.P., 2011. Hydrogen isotopes in individual alkenones from the Chesapeake Bay estuary. Geochimica et Cosmichimica Acta, 75, 7552–7565.

Sessions, A.L., Burgoyne, T.W., Schimmelmann, A., Hayes, J.M., 1999. Fractionation of hydrogen isotopes in lipid biosynthesis. Organic Geochemistry, 30, 1193-1200.

Suc J.-P., Fauquette S.**,** Bessedik M., Bertini A., Zheng Z., Clauzon G., Suballyova D., Diniz F., Quézel P., Feddi N., Clet M., Bessais E., Bachiri Taoufiq N., Méon H., Combourieu-Nebout , N., 1999. Neogene vegetation changes in West European and West circum-Mediterranean areas. In "Hominid Evolution and Climatic Change in Europe", Vol. 1 : "Climatic and Environmental Change in the Neogene of Europe", Agusti J., Rook L. et Andrews P. Edit., Cambridge University Press, 378-388.

Speelman, E.N, Sewall, J.O., Noone, D., Huber, M., von der Heydt, A., Sinninghe Damsté, J., Reichart, G.J., 2010. Modeling the influence of a reduced equator-to-pole sea surface temperature gradient on the distribution of water isotopes in the Early/Middle Eocene. Earth and Planetary Science Letters, 298, 57-65.

Speranza, G., Cosentino, D., Tecce, F., Faccenna, C., 2013, Paleoclimate reconstruction during the Messinian evaporative drawdown of the Mediterranean Basin: Insights from microthermometry on halite fluid inclusions, Geochemistry Geophysics Geosystems, 14, doi:10.1002/2013GC004946.

Stoica, M., Lazar, I., Krijgsman, W., Vasiliev, I., Jipa, D.C. and Floroiu, A., 2013. Palaeoenvironmental evolution of the East Carpathian foredeep during the late Miocene - early Pliocene (Dacian Basin; Romania). Global and Planetary Change, 103, 135-148.

Stoica, M., Krijgsman, W., Fortuin, A.R., Gliozzi, E., 2015. Paratethyan ostracods in the Spanish Lago-Mare: more evidence for interbasinal exchange at high Mediterranean sea level, Palaeogeography, Palaeoclimatology, Palaeoecology, 441, 854-870.

Thiel, V., Jenisch, A., Landmann, G., Reimer, A., Michaelis, W., 1997. Unusual distributions of long-chain alkenones and tetrahymenol from the highly alkaline Lake Van, Turkey. Geochimica et Cosmochimica Acta, 61, 2053-2064.

Tipple, B.J. and Pagani, M., 2010. A 35 Myr North American leaf-wax compound-specific carbon and hydrogen isotope record: Implications for C_4 grasslands and hydrologic cycle dynamics. Earth and Planetary Science Letters, 299, 250-262.

van der Meer, M.T.J., Baas, M., Rijpstra, I.C.,, Marino, G., Rohling, E. J., Sinninghe Damsté, J.S., Schouten, S. 2007. Hydrogen isotopic compositions of long-chain alkenones record freshwater flooding of the Eastern Mediterranean at the onset of sapropel deposition. Earth and Planetary Science Letters, 262, 594–600.

van der Meer, M.T.J., Sangiorgi, F., Baas, M., Brinkhuis, H., Sinninghe Damsté, J.S., Schouten, S. 2008. Molecular isotopic and dinoflagellate evidence for Late Holocene freshening of the Black Sea. Earth and Planetary Science Letters, 267, 426–434.

van der Meer, M.T.J, Benthien, A., French, K.L., Epping, E., Zondervan, I., Reichart, G.J., Bijma, J., Sinninghe Damsté, J.S., Schouten, S. 2015. Large effect of irradiance on hydrogen isotope fractionation of alkenones in *Emiliania huxleyi*. Geochimica et Cosmochimica Acta, 160, 16-24.

van Baak, G. C., Radionova, E. P., Golovina, L. A., Raffi, I., Kuiper, K. F., Vasiliev, I., Krijgsman, W. 2015. Messinian events in the Black Sea. Terra Nova, 27 (6), 433-441.

Vasiliev, I., Reichart, G.J., Davies, G., Krijgsman, W., Stoica, M. (2010). Strontium isotope ratios of the Eastern Paratethys during the Mio-Pliocene transition; Implications for interbasinal connectivity, Earth and Planetary Science Letters, 292, 123-131.

Vasiliev I., Iosifidi A.G., Khramov A.N., Krijgsman W., Kuiper, K.F., Langereis C.G., Popov V.V., Stoica M., Tomsha V.A., Yudin S.V., 2011. Magnetostratigraphy and radiometric dating of upper Miocene - lower Pliocene sedimentary successions of the Black Sea Basin (Taman Peninsula, Russia), Palaeogeography, Palaeoclimatology, Palaeoecology, 310, 163-175.

Vasiliev, I., Reichart, G.J., Krijgsman, W., 2013. Impact of the Messinian Salinity Crisis on Black Sea hydrology – Insights from hydrogen isotopes on molecular biomarkers, Earth and Planetary Science Letters, 362, 272-282.

Vasiliev, I., Reichart, G.-J., Grothe, A., Sinninghe Damsté, J.S., Krijgsman, W., Sangiorgi, F., Weijers, J.W.H., van Roij, L., 2015. Recurrent phases of drought in the upper Miocene of the Black Sea region, Palaeogeography, Palaeoclimatology, Palaeoecology, 423, 18-31.

Volkman, J.K., Eglinton, G., Corner, E.D.S., Forsberg, T.E.V., 1980. Long chain alkenes and alkenones in the marine coccolithophorid *Emiliania huxleyi*. Phytochemistry, 19, 2619-2622.

Table 1. δD isotopes measured on long chain C_{29} and C_{31} n-alkanes from Monto Tondo and Eraclea Minoa (MSC stages 1 and 3). The δD_{precip} is calculated for a 'wet' climate using Sachse et al. (2006) and for a 'dry' climate using Feakins and Sessions, (2010). Average, standard deviation (STDEV) and standard error of the means (SEM) are listed; n.d denotes levels where the $\delta^{13}C$ or δD could not determine.

Table 2. δD isotopes measured on alkenones from Realmonte and Eraclea Minoa (MSC stages 2 and 3). The δD of the source waters (δD_{water}) were calculated using the relations of Englebrecht and Sachs (2005) for C_{37} and C_{38} separately and Schwab &Sachs (2011) for $C_{37:2}$, $C_{37:3}$, $C_{38:2}$ and $C_{38:3}$ separately. See also the captions of table 1.

Figure captions

Figure 1. Palaeogeographic map of the late Miocene, showing the Mediterranean and Paratethys areas on the presented day land configuration. Major rivers draining into the Mediterranean and Paratethys (former sea of Eurasia) are indicated (modified after Vasiliev et al. 2013 and 2015). The values of the present day precipitation $\delta D_{precipitation}$ are reported according to IAEA (2001) and their locations marked by the white circle. Long-term means were calculated by selecting yearly means in which isotope content have been measured at least in 75% of the precipitation for that year and at least over eight months (IAEA, 2001).

The locations of Taman peninsula (TM) with Zheleznyi Rog section used in Vasiliev et al., (2013) and Deep Sea Drilling Project 42B (Hole 380A) used in Vasiliev et al., (2015) are represented by yellow triangles.

Figure 2. Chronostratigraphy of Late Miocene to Early Pliocene with MSC events in the Mediterranean (modified from CIESM, 2008; Manzi et al., 2013, Roveri et al., 2014a) and correlations to the oxygen isotope curves of the Atlantic margin of Morocco (Hilgen et al., 2007). PLG, Primary Lower Gypsum; RLG, Resedimented Lower Gypsum; UG, Upper Gypsum; CdB, Calcare di Base. **MSC stage 1** corresponds to deposition of euxinic shales and dolomites in the intermediate basins and to the deposition of the PLG in the shallow basins. **MSC stage 2** corresponds to Resedimented Lower Gypsum and halite in the intermediate basins while in the shallow basins this stage 2 of MSC is marked by a hiatus of variable amplitude. **MSC stage 3** corresponds to Upper Gypsum and Lago Mare in the intermediate basins. The hiatus of variable amplitude starting in the MSC 2 continues during the MSC stage 3 in some locations in the shallow basins.

Figure 3. Representative chromatograms of biomarker fractions of representative sedimentary samples of the Monto Tondo, Realmonte and Eraclea Minoa (MSC stages 1, 2 and 3). In the left hand side are the represented the a-polar fractions (a, c, e, g, i, and k); note the *n*-alkanes with a distinctly odd (green) over even (orange) carbon-number predominance. In the right hand side are the ketone fractions (b, d, f, h, j and l). Note the similarity of the alkenone distribution in both sediments although they belong to levels with the distinctly different $\delta D_{alkenone}$.

Figure 4. Cross plots of δD measured on *n*-alkanes and long chain alkenones from Monto Tondo and Eraclea Minoa (MSC stages 1 and 3). The numbers in italics indicate stratigraphic levels (in mbsf) of samples further from the correlation lines. Comparison of measured δD on C_{29} and δD on C_{31} *n*-alkanes and of measured δD on C_{37} and δD on C_{38} alkenones.

Figure 5. δD isotopes of C_{29} and C_{31} *n*-alkanes and C_{37} and C_{38} long chain alkenones recorded in the composite of Monte Tondo, Realmonte and Eraclea Minoa sections (MSC stages 1, 2 and 3). Between the *n*-alkanes and alkenones records is the schematic representation of the Messinian Salinity Crisis stages (1, 2 and 3) coinciding with Monte Tondo, Real Monte and Eraclea Minoa. In the upper part of the y axes are the δD scales are indicated possible causes for depleted versus enriched $\delta D_{n\text{-alkanes}}$ and $\delta D_{alkenones}$ values recorded. Blue line indicate the values recorded in the present day setting for the *n*-alkanes in the lakes close to the actual location of the studied sections (Sachse et al., 2006) and in the alkenones from the Mediterranean in the recent times (Van der Meer et al., 2007). Error bars are based on the standard deviation of the complete set of replicate analyses and indicate standard errors of the mean. To not complicate the figure we refrain from presenting the calculated values for the $\delta D_{precipitation}$ in the two cases exposed in the main text and enumerated in table 1 (European 'humid' temperate and 'arid' climates).

Figure 6. Comparison of the $\delta D_{n\text{-alkanes}}$ and $\delta D_{alkenones}$ records of Mediterranean (Monte Tondo, Realmonte and Eraclea Minoa) and of Paratethys (DSDP Hole 380A and

Zheleznyi Rog of Taman Peninsula). On the left side Mediterranean and Paratethys time scales are presented next to oxygen isotope record. TG indicates glacial–interglacial marine stages. Events of the Messinian Salinity Crisis and regional Black Sea (i.e. Paratethys) stage names are listed. The age model is according to Krijgsman et al. (2010). The foraminifer symbol indicates the level of marine transgression into Paratethys. The Mediterranean values in red are from this study and substantiated with $\delta D_{n\text{-alkanes}}$ and $\delta D_{alkenones}$ data from Vasiliev et al., 2013, 2015 and δD water estimated by Andersen et al., 2001. Scenarios of Mediterranean-Paratethys-Atlantic connections at important moments of MSC (for consistency with the succession of the events read from the bottom of the figure to the top one, form panels c to a). a) 'Lago Mare'/ Gypsum deposition (stage 3) of the MSC under the assumption that an intermittent influx from the ocean (via Atlantic) existed at a not significant Mediterranean Sea level drop, as suggested by marine fishes and marked with the purple arrow (Carnevale et al., Roveri et al., 2014b). The probable influx of Paratethys waters, as suggested by 'Lago Mare' type of biota is marked by blue arrow. Both influxes into Mediterranean, from Atlantic and from Black Sea, are possible; b) Halite deposition during the climax of the MSC (stage 2) under the assumption that a moderate Mediterranean Sea level drop existed. Still, excess precipitation in the Black Sea could result in overspill into Mediterranean. c) PLG deposition (stage 1) of the MSC. Remark the ~40 ‰ difference between the $\delta D_{n\text{-alkanes}}$ of Upper Gypsum and $\delta D_{n\text{-alkanes}}$ of Lower Primary Gypsum. Remark more than 50 ‰ variation in the $\delta D_{alkenones}$ between values recorded for the halite (stage 2) and 'Lago Mare'/ Gypsum deposition (stage 3). HSL and LSL stand for high or low sea level respectively.

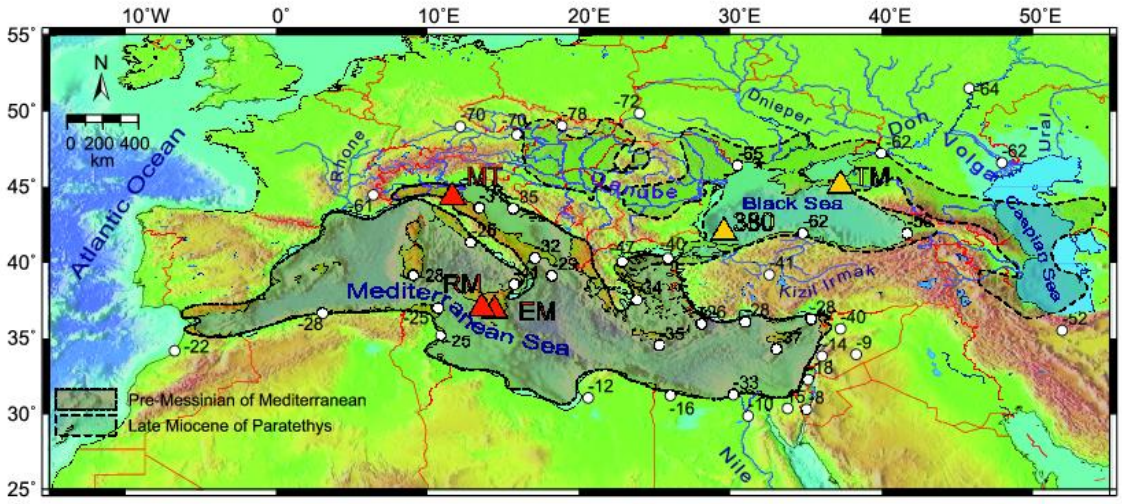

Figure 1

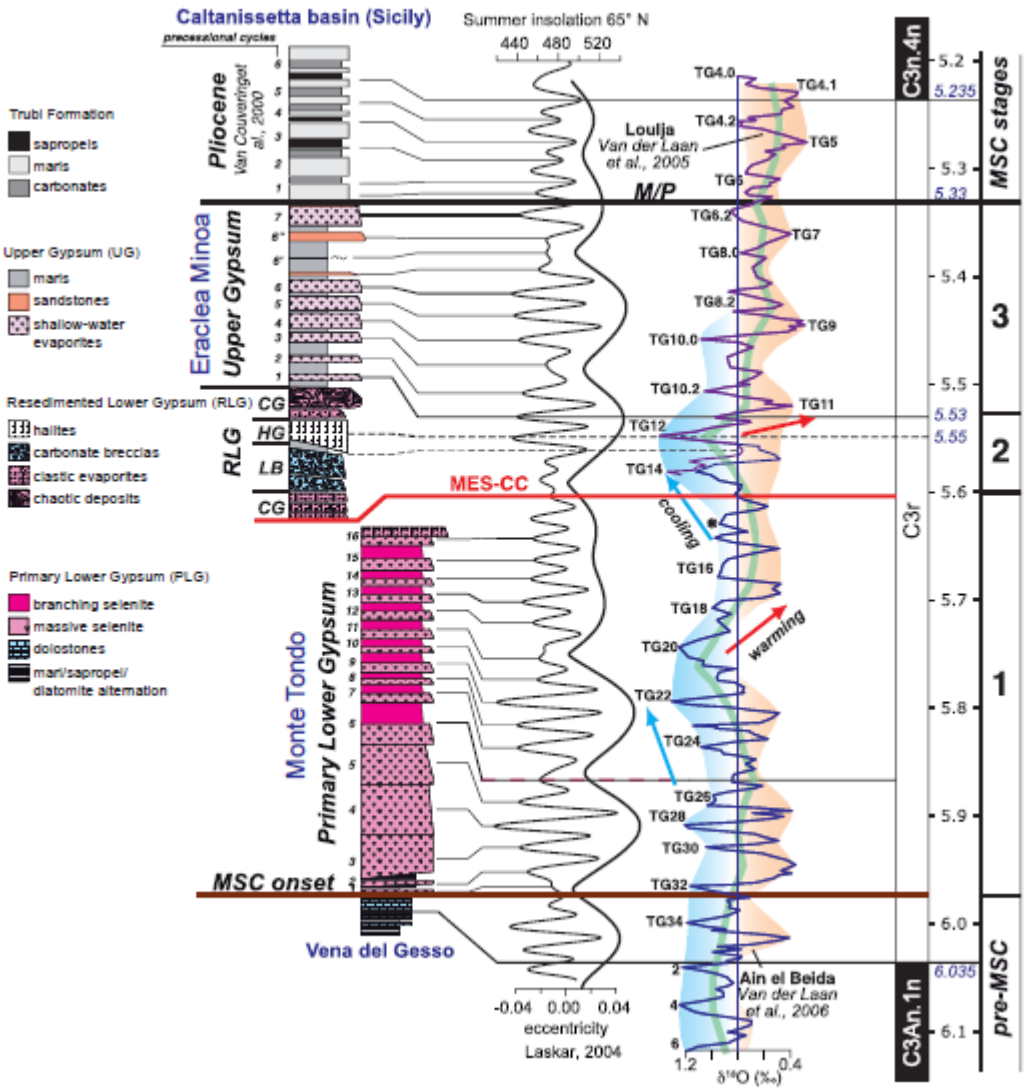

Figure 2

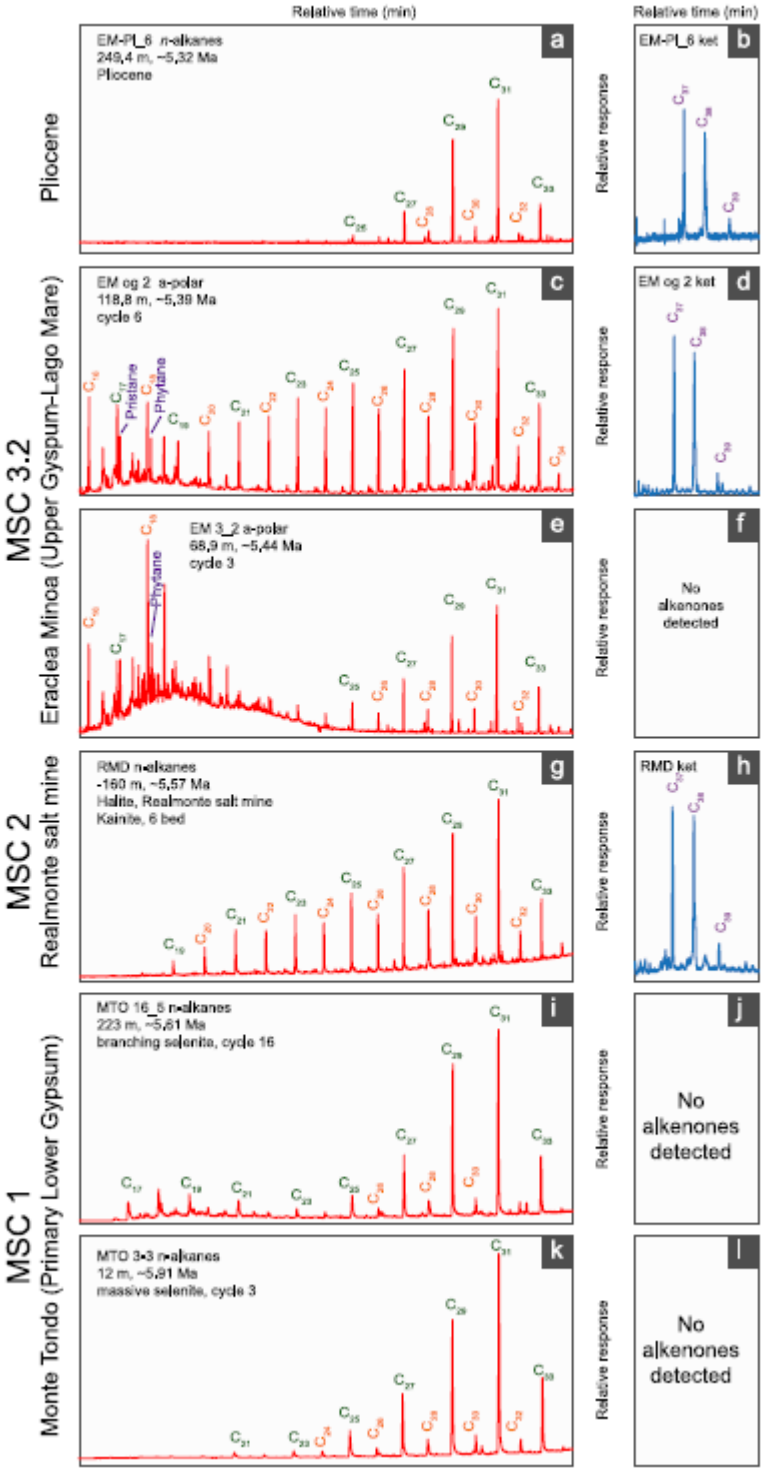

Figure 3

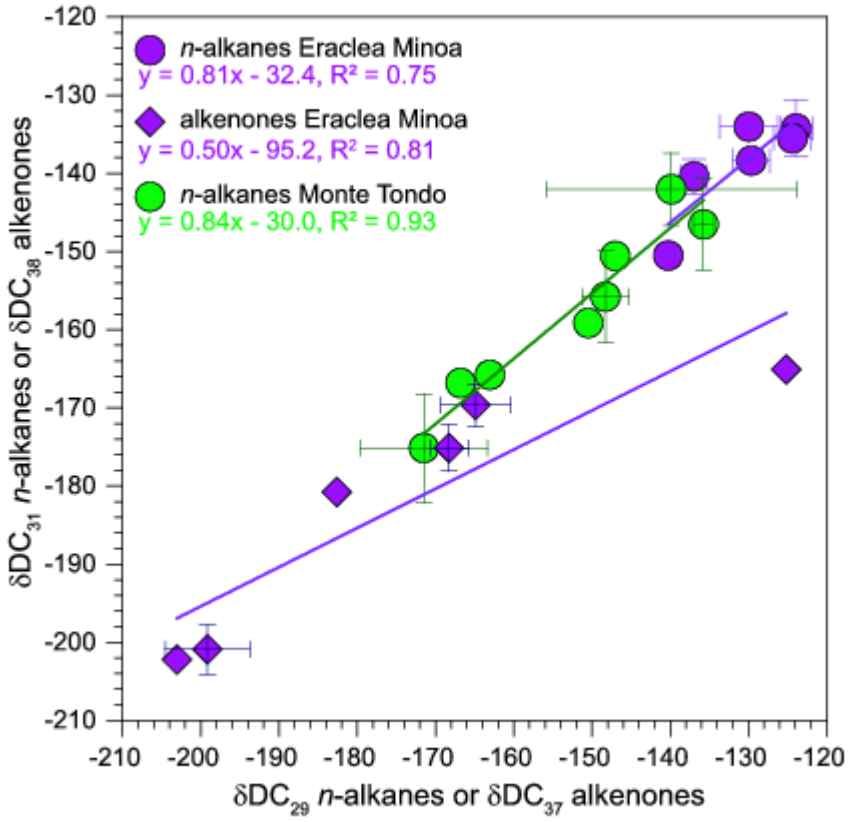

Figure 4

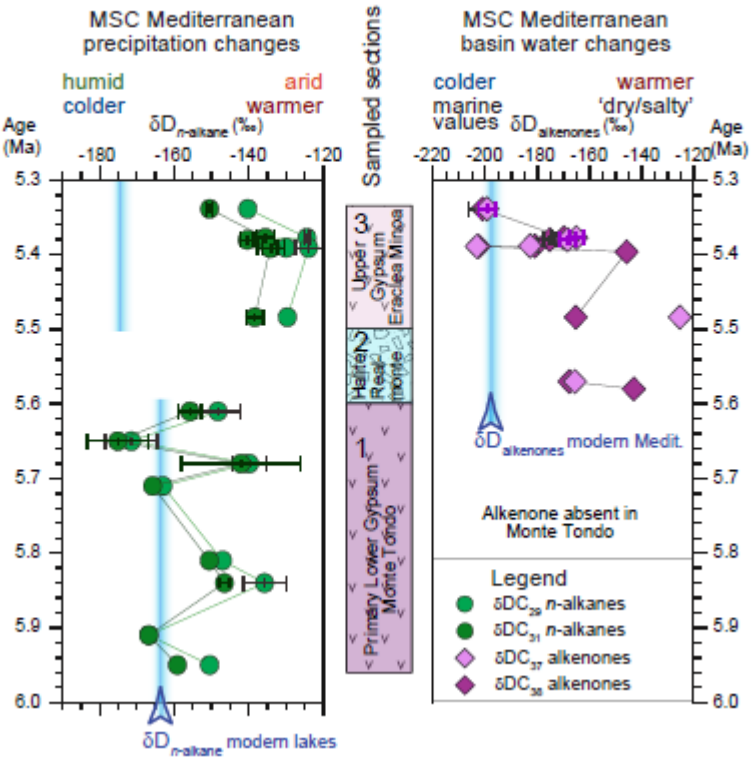

Figure 5

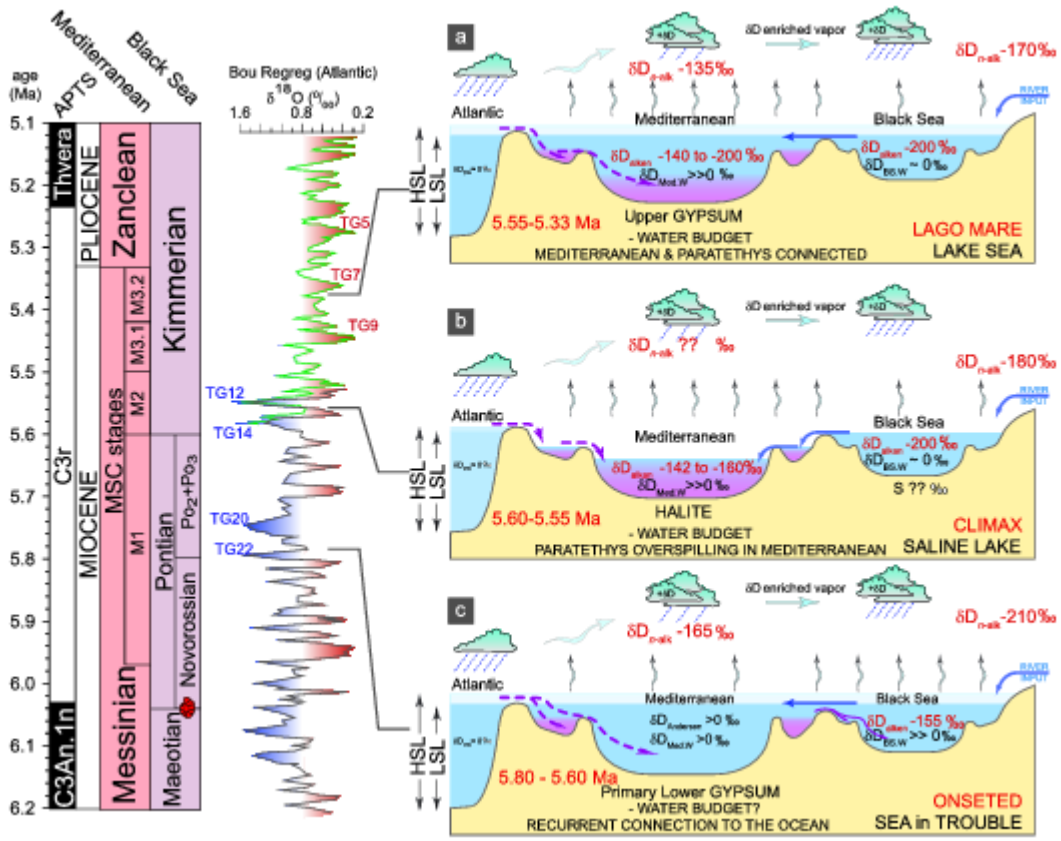

Figure 6

Table 1

Sample code	Level (m)	Rock type	Age (Ma)	δD_{nC29} (‰)	N	STDEV	δDpp from δ_{DnC29} (‰)		δDnC31 (‰)	N	STDEV	δDpp from δ_{DnC31} (‰)		CPI	ACL
							WET	DRY				WET	DRY		
MTO 1_3	2.5	massive selenite	5.969	-150.5	1		-23.5	-62.3	-159.1	1		-33.5	-71.9	6.0	29.6
MTO 3_3a	12	massive selenite	5.929	-166.8	1		-42.3	-80.4	-166.8	1		-42.3	-80.4	5.8	29.9
MTO 6_4a	103	banded selenite	5.897	-135.7	2	5.8	-6.6	-46.1	-146.5	2	1.3	-19.0	-58.0	3.0	28.8
MTO 7_4_2	126	banded selenite	5.837	-147.0	1		-19.6	-58.5	-150.6	1		-23.6	-62.4	5.8	30.1
MTO 12_4	173	banded selenite	5.721	-163.1	1		-38.0	-76.2	-165.8	1		-41.1	-79.2	5.2	28.6
MTO 13_5	189.5	branching selenite	5.702	-139.9	2	4.6	-11.3	-50.6	-142.0	2	16.0	-13.8	-53.0	6.0	29.6
MTO 15_2	205	limestone	5.663	-171.5	6	6.9	-47.7	-85.5	-175.1	6	8.2	-51.9	-89.5	5.9	29.2
MTO 16_5	223	branching selenite	5.643	-148.3	2	5.9	-21.0	-59.9	-155.8	2	3.0	-29.6	-68.2	7.9	29.8
EM_og_15	4.5	banded selenite	5.53	-129.6	1		0.4	-39.3	-138.4	2	2.4	-9.6	-49.0	n.d.	n.d.
EM-og1	118	marl	5.405	-123.9	2	3.6	7.0	-33.0	-134.3	2	2.0	-4.9	-44.4	2.2	28.9
EM2	118.8	marl	5.416	-129.9	1		0.1	-39.7	-134.0	2	3.7	-4.6	-44.2	2.5	29.2
EM6'_26	159.5	marl	5.394	-137.0	2	2.2	-8.0	-47.4	-140.4	2	1.7	-12.0	-51.2	2.3	29.4
EM6"_7	170	marl	5.386	-124.4	3	0.7	6.5	-33.5	-135.5	3	2.4	-6.3	-45.8	1.7	29.1
EM8_6	238.2	marl	5.333	-140.2	1		-11.8	-51.0	-150.5	4	0.9	-23.6	-62.4	3.7	29.8

Table 2

Sample	Depth (m)	Age (Ma)	δD_{C37} (‰)	N	STDEV	δD_{C38} (‰)	N	STDEV	dD_w Englebrecht & Sachs (2005)		dD_w Schwab & Sachs (2011)			
									C37	C38	$\delta D_{C37:2}$	$\delta DC_{37:3}$	$\delta DC_{38:2}$	$\delta DC_{38:3}$
EM_og_15	4.5	5.4837	-125.2	1		-165.1	1		136	91	66	67	11	33
EM Ra	112.5	5.3962	n.d	n.d.		-145.6	1		n.d.	117	n.d	n.d	40	58
EM og 09	128	5.3888	-203.0	1		-202.2	1		30	41	-33	-66	-44	-15
EM12ket	128.5	5.3883	-182.6	4		-180.8		1	58	70	-7	-31	-12	13
EM6'_26	159.5	5.3801	-168.3	5	2.97	-175.1	4	2	78	78	11	-7	-4	20
EM6''_7	170	5.3774	-164.9	3	2.70	-169.6	5	4	82	85	16	-1	4	27
EM8_6	238.2	5.3387	-199.2	1	3.20	-200.9	3	5	35	43	-28	-59	-42	-13
RMI	-106	5.58	n.d.			-142.8	1		n.d.	121	n.d.	n.d.	44	62
RMD	-160	5.57	-165.5	1		-167.6	1		81	88	15	-2	7	30